Acta Crystallographica Section D
Biological Crystallography
ISSN 0907-4449

Inhibition of D-xylose isomerase by polyols: atomic details by joint X-ray/neutron crystallography

Andrey Kovalevsky,[a]* B. Leif Hanson,[b] Sax A. Mason,[c] V. Trevor Forsyth,[c,d] Zoe Fisher,[a] Marat Mustyakimov,[a,f] Matthew P. Blakeley,[c] David A. Keen[e] and Paul Langan[f]

[a]Bioscience Division, Los Alamos National Laboratory, PO Box 1663, MS M888, Los Alamos, NM 87545, USA, [b]Department of Chemistry, University of Toledo, 2801 West Bancroft Street, Toledo, OH 43606, USA, [c]Institut Laue–Langevin, 6 Rue Jules Horowitz, 38042 Grenoble, France, [d]EPSAM/ISTM, Keele University, Staffordshire, England, [e]ISIS Facility, Rutherford Appleton Laboratory, Harwell Science and Innovation Campus, Didcot, Oxon OX11 0QX, England, and [f]Biology and Soft Matter Division, Oak Ridge National Laboratory, PO Box 2008, MS 6475, Oak Ridge, TN 37831, USA

Correspondence e-mail: ayk@lanl.gov

Received 10 April 2012
Accepted 30 May 2012

PDB References: D-xylose isomerase, complex with Mn^{2+} and xylitol, 4duo; complex with Ni^{2+} and sorbitol, 4dvo.

D-Xylose isomerase (XI) converts the aldo-sugars xylose and glucose to their keto analogs xylulose and fructose, but is strongly inhibited by the polyols xylitol and sorbitol, especially at acidic pH. In order to understand the atomic details of polyol binding to the XI active site, a 2.0 Å resolution room-temperature joint X-ray/neutron structure of XI in complex with Ni^{2+} cofactors and sorbitol inhibitor at pH 5.9 and a room-temperature X-ray structure of XI containing Mg^{2+} ions and xylitol at the physiological pH of 7.7 were obtained. The protonation of oxygen O5 of the inhibitor, which was found to be deprotonated and negatively charged in previous structures of XI complexed with linear glucose and xylulose, was directly observed. The Ni^{2+} ions occupying the catalytic metal site (M2) were found at two locations, while Mg^{2+} in M2 is very mobile and has a high *B* factor. Under acidic conditions sorbitol gains a water-mediated interaction that connects its O1 hydroxyl to Asp257. This contact is not found in structures at basic pH. The new interaction that is formed may improve the binding of the inhibitor, providing an explanation for the increased affinity of the polyols for XI at low pH.

1. Introduction

D-Xylose isomerase (XI) is an intracellular metalloenzyme that is expressed by some anaerobic bacteria, fungi and plants (Bhosale *et al.*, 1996; Parachin & Gorwa-Grauslund, 2011). It can convert D-glucose to D-fructose and has been extensively used over the past two decades for the production of starch-based high-fructose corn syrup (Bhosale *et al.*, 1996; van Maris *et al.*, 2007). Its natural substrate is the aldo-pentose sugar D-xylose, which the enzyme converts to the keto analog D-xylulose. In recent years, XI has also been introduced into the yeast *Saccharomyces cerevisiae* to improve the utilization of D-xylose during the fermentation of lignocellulosic hydrolysates to produce bioethanol; the yeast cannot naturally assimilate hemicellulose-derived D-xylose, but can catabolize D-xylulose (van Maris *et al.*, 2007; Matsushika *et al.*, 2009; Van Vleet & Jeffries, 2009; Madhavan *et al.*, 2009). Nonetheless, XI is a low-efficiency enzyme (k_{cat}/K_m for xylose is $\sim 10^3\ M^{-1}\ s^{-1}$) and is prone to strong inhibition by the polyols xylitol and sorbitol, which are the reduced analogs of xylose and glucose, respectively (Fig. 1), causing diminished performance of the ethanol-fermenting yeast (van Bastelaere *et al.*, 1991; Tanino *et al.*, 2010).

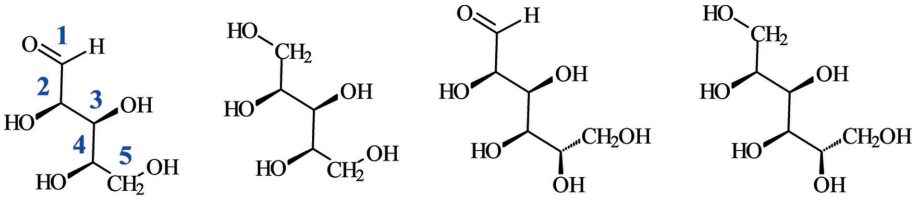

Figure 1
Chemical diagram of the linear forms of aldoses and their corresponding polyols.

XI folds into the well known $(\alpha/\beta)_8$ TIM-barrel tertiary structure of triose isomerase (Carrell *et al.*, 1989). It is activated by the formation of a homotetramer and the subsequent binding of two divalent-metal cofactors to each of the four active sites. The pH range for optimal activity is 7–8. Loss of activity at low pH is thought to proceed by the expulsion of both metal cations from the active site and the dissociation of the tetramer (Jänis *et al.*, 2008). Previously, we used joint X-ray/neutron (XN) crystallography to reveal that when the pH is below 6 one of the metal-binding sites (M1) of apo XI is protonated by a single H atom (Kovalevsky *et al.*, 2011). H atoms are difficult to see in the active site of XI using X-rays, but can be easily located using neutrons (Fenn *et al.*, 2004; Toteva *et al.*, 2011). In fact protons (H^+) are completely invisible to X-rays, even at subatomic resolution. This protonation causes the M1 site to collapse, preventing metal binding, and therefore providing a possible explanation for the resulting enzyme inactivation (Kovalevsky *et al.*, 2011). XI is activated by only four divalent-metal species, Mg^{2+}, Mn^{2+}, Co^{2+} and Fe^{2+}, of which Mg^{2+} is the physiological metal in most organisms, while Mn^{2+} appears to activate *Escherichia* sp. XI better (van Bastelaere *et al.*, 1991; Callens *et al.*, 1986). All other metals, including transition, alkali-earth and rare-earth species, inhibit the catalytic activity of XI (Callens *et al.*, 1986; Sudfeldt *et al.*, 1990).

Several mechanisms have been proposed for the conversion of an aldo-sugar into its keto isomer by XI; they agree on the major stages of the reaction, but differ in the details (Whitlow *et al.*, 1991; Allen *et al.*, 1994; Carrell *et al.*, 1994; Asbóth & Náray-Szabó, 2000; Fenn *et al.*, 2004). In the first stage, the α-anomer of a cyclic substrate binds to the structural metal (site M1) and the sugar ring is opened to produce a linear intermediate (aldehyde form; Fig. 1) and to prime the substrate for the isomerization stage. One path for the subsequent isomerization stage is *via* a hydride shift between C atoms C1 and C2 of the linear sugar and may be initiated by movement of the catalytic metal (site M2) closer to the sugar to coordinate its hydroxyl groups at C1 and C2 (Asbóth & Náray-Szabó, 2000; Fenn *et al.*, 2004). H atoms play critical roles during the conversion reaction and must be moved between water, substrate and active-site residues at different stages.

Our recent XN studies of XI from *Streptomyces rubiginosus* involved mapping the location of H atoms, and therefore their possible movement, in the active site at different stages of the catalyzed reaction (Katz *et al.*, 2006; Kovalevsky *et al.*, 2008, 2010). This suggested modification of the previous proposals for the ring-opening and isomerization stages. Moreover, the XN structure of XI in complex with nickel metal cofactors and linear glucose provided unambiguous evidence that ring opening results in the production of an aldehyde group at C1 and that no hydration of the carbonyl occurs in the enzyme-bound state (Kovalevsky *et al.*, 2010).

The chemical structures of polyols such as xylitol and sorbitol are similar to those of the linear forms of xylose and glucose (Fig. 1), differing only in the substitution of an aldehyde group by a hydroxymethylene moiety at C1 (Madsen *et al.*, 2003). Xylitol and sorbitol are therefore good mimics of the linear sugars and have a high affinity for binding in the XI active site. In fact, solution kinetics have demonstrated that the inhibition of XI activity by xylitol (K_i) is about one order of magnitude better than the affinity of the active site (K_m) for cyclic xylose (van Bastelaere *et al.*, 1991). Moreover, binding of xylitol improves dramatically when the pH is lowered below 6. As xylitol is enzymatically synthesized from xylose in *S. cerevisiae* by a nonspecific aldose reductase, it can efficiently inhibit XI in the acidic (pH ∼5) cytosol of yeast. Determining in detail how a polyol inhibitor binds to the XI active site at low pH would be of great value in engineering XI variants with a lower binding affinity for xylitol.

Here, we report the 2.0 Å resolution XN room-temperature structure of XI from *S. rubiginosus* in complex with two Ni^{2+} cofactors and sorbitol at pH 5.9, which we refer to as XI-Ni_2-Sorbitol_xn (PDB entry 4dvo). Ni^{2+} was used to unambiguously locate the metals in the XI active site and to compare its binding in complexes with polyol and with linear glucose. D has a positive neutron scattering length of 6.671 fm, which is similar to those of C, N and O, while H scatters neutrons negatively (−3.741 fm) with a strong incoherent component that adds to the scattering background in diffraction images. We therefore subjected our crystals to H/D exchange to replace H atoms in water and on the OH, NH and SH groups of the enzyme with D, while the CH groups remained non-exchanged. The sorbitol used was perdeuterated. In addition, we report a 2.0 Å resolution room-temperature X-ray structure of XI in complex with natural Mg^{2+} cofactors and xylitol inhibitor (XI-Mg_2-Xylitol_x; PDB entry 4duo) at the physiological pH of 7.7 to compare the binding modes of the polyols at different pH values.

2. Materials and methods

2.1. General information

XI (from *S. rubiginosus*; molecular weight 172 kDa) was purchased from Hampton Research (Aliso Viejo, California, USA). Sample preparation and crystallization were performed as described previously (Kovalevsky *et al.*, 2010, 2011). Perdeuterated sorbitol (D-[d_{14}]-sorbitol) was purchased from

Table 1
Room-temperature X-ray crystallographic data-collection and refinement statistics for XI-Mg_2-Xylitol_x (pH = 7.7).

Values in parentheses are for the highest resolution shell. Data were collected from one crystal.

PDB entry	4duo
Data collection	
Space group	*I*222
Unit-cell parameters (Å, °)	a = 93.79, b = 99.62, c = 102.83, $\alpha = \beta = \gamma$ = 90
Resolution (Å)	71.6–2.00 (2.11–2.00)
R_{merge}†	0.063 (0.113)
$\langle I/\sigma(I)\rangle$	16.7 (10.6)
Completeness (%)	96.0 (95.0)
Multiplicity	2.7 (2.7)
No. of reflections measured	85647
No. of unique reflections	31472
Refinement	
Resolution (Å)	10–2.0
No. of reflections	29644
R_{work}‡/R_{free}§	0.145/0.199
No. of atoms	
Protein	3061
Ligand/ion	12
Water	228
B factors (Å^2)	
Protein	22.1
Ligand/ion	19.4
Water	34.1
R.m.s. deviations	
Bond lengths (Å)	0.007
Bond angles (°)	0.023

† $R_{merge} = \sum_{hkl}\sum_i |I_i(hkl) - \langle I(hkl)\rangle| / \sum_{hkl}\sum_i I_i(hkl)$. ‡ $R_{work} = \sum_{hkl} ||F_{obs}| - |F_{calc}|| / \sum_{hkl} |F_{obs}|$. § R_{free} is calculated in the same way as R_{work} for data omitted from refinement (5% of reflections for all data sets).

Table 2
Room-temperature neutron crystallographic data-collection and joint XN refinement statistics for XI-Ni_2-Sorbitol_xn (pH = 5.9).

Values in parentheses are for the highest resolution shell. Data were collected from one crystal.

PDB entry	4dvo
Data collection	
Space group	*I*222
Unit-cell parameters (Å, °)	a = 94.06, b = 99.43, c = 102.80, $\alpha = \beta = \gamma$ = 90
Resolution (Å)	49.72–2.00 (2.10–2.00)
R_{merge}	0.154 (0.408)
$\langle I/\sigma(I)\rangle$	7.6 (1.8)
Completeness (%)	93.0 (90.0)
Multiplicity	4.0 (2.4)
No. of reflections measured	175145 (9607)
No. of unique reflections	30585 (3983)
Data-rejection criterion	No observation and $\lvert F\rvert = 0$
Joint XN refinement	
Resolution (neutron) (Å)	20–2.0
Resolution (X-ray) (Å)	20–1.55
No. of reflections (neutron)	30162
No. of reflections (X-ray)	64311
Data-rejection criterion	$\lvert F\rvert < 2.0$
R_{work}/R_{free} (neutron)	0.190/0.214
R_{work}/R_{free} (X-ray)	0.194/0.204
No. of atoms	
Protein including H and D	5977
Ligand/ion	29
Water	864 [266 D_2O molecules]
B factors (Å^2)	
Protein	24.5
Ligand/ion	27.6
Water	42.6
R.m.s. deviations	
Bond lengths (Å)	0.006
Bond angles (°)	0.921

Omicron Biochemicals Inc. Crystals were sealed in quartz tubes crafted into hourglass shapes and sealed with wax. The lower part of each tube was filled with 400–500 µl $(ND_4)_2SO_4$/MES (or HEPES) solution made with 100% D_2O.

2.2. X-ray crystallography

All data sets were collected at room temperature using a Rigaku FR-E generator equipped with an R-AXIS VI++ detector. Diffraction data were integrated and scaled using the *CrystalClear*/*d*TREK* software (Pflugrath, 1999) and the structures were refined using *SHELX* (Sheldrick, 2008). For joint XN structure refinement the X-ray data were collected from crystals that were taken from the same crystallization drops that provided the larger crystals for the neutron data set and were exchanged with D_2O in a similar way as was performed for the neutron studies. A summary of the X-ray crystallographic data for XI-Mg_2-Xylitol_x is given in Table 1.

2.3. Neutron crystallography

Monochromatic neutron data were collected from XI-Ni_2-Sorbitol_xn crystals to 2.0 Å resolution at room temperature on beamline D19 at the Institut Laue–Langevin (ILL) using ω step-scans (0.07° steps with an exposure time of 100 s per step) and a wavelength of 2.422 Å. The data were processed using the ILL program *RETREAT* (Wilkinson *et al.*, 1988), corrected for effective absorption and then merged using *SCALA* from the *CCP*4 suite of programs (Winn, 2011). A summary of the experimental data for XI-Ni_2-Sorbitol_xn is given in Table 2.

2.4. Joint XN structure refinement

The joint XN structure XI-Ni_2-Sorbitol_xn was determined using *nCNS* (Adams *et al.*, 2009). Rigid-body refinement was followed by several cycles of positional, atomic displacement parameter and occupancy refinement and then by water (D_2O) building. Side-chain conformations, the orientations of hydroxyl groups, the protonation states of His and Lys residues and the orientations of water (D_2O) molecules were then examined and altered, if necessary, based on the $2F_o - F_c$ and difference $F_o - F_c$ neutron scattering density maps. The level of H/D exchange at labile positions of the enzyme was refined. A complete description of the refinement process can be found elsewhere (Kovalevsky *et al.*, 2010, 2011). Before depositing the final structures in the PDB, a script was run that converts the record for the coordinates of a labile D atom into two records corresponding to an H and a D atom partially occupying the same coordinates, both with positive partial occupancies that add up to unity. The refinement statistics are represented in Table 2. The structures were built and manipulated with *Coot* (Emsley *et al.*, 2010), while the figures were generated using *PyMOL* v.1.4 (Schrödinger LLC).

3. Results and discussion

All of the D atoms of sorbitol could be clearly observed in the nuclear density map (Fig. 2*a*). The D atom on O5 is visible as a strong peak in the OMIT $F_o - F_c$ nuclear density map (Fig. 2*b*). The protonated O5 donates its D atom in a hydrogen bond to a water molecule, while accepting another hydrogen bond from the doubly protonated His54. This is in contrast to our previous studies of XI with linear glucose (Kovalevsky *et al.*, 2010) and linear xylulose (Kovalevsky *et al.*, 2008), in which we found O5 to be deprotonated, negatively charged and locked in a strong salt bridge to the protonated positively charged catalytic His54 after ring opening. In these previous studies we also observed the deprotonated O5 accepting a D atom from, rather than donating a D atom to, a D_2O molecule in a hydrogen bond. The direct observation of a D atom on O5 of sorbitol in this study and the absence of a D atom after ring opening in our previous studies would appear to clearly validate our XN crystallographic method.

The Ni^{2+} ion at site M1 coordinates the O2 and O4 hydroxyl O atoms of sorbitol (Fig. 3*a*). M2 has two well defined subsites 2a and 2b, which are almost 2 Å apart and have occupancies of 0.5 each. We have previously observed such an arrangement of nickel cations in the complex of XI with linear glucose (Kovalevsky *et al.*, 2010). The observation of the two subsites for Ni^{2+} in the current structure may indicate that M2 naturally has a subsite 2b, rather than this site being generated after ring opening as we had suggested previously. In XI-Ni_2-Sorbitol_xn M2a is over 3 Å away from O1 and O2, but M2b is within coordinating distance (<2.4 Å) of the O atoms. The O1 and O3 hydroxyl O atoms of the inhibitor make water-mediated contacts with Asp257 and the protonated Lys289, respectively (Fig. 3*a*). We have previously observed Lys289 to be protonated at low pH in apo XI.

To understand the differences in inhibitor binding at different pH values, we also obtained a 2.0 Å resolution room-temperature X-ray structure of XI in complex with Mg^{2+} and

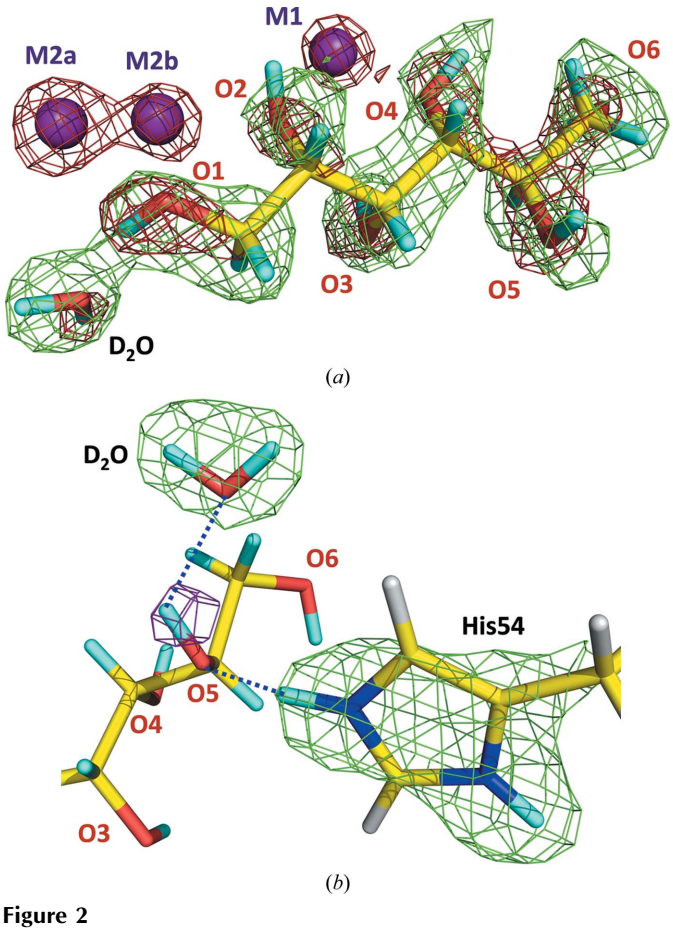

Figure 2
(*a*) Superposition of the $2F_o - F_c$ electron-density maps (red; 2σ contour level for sorbitol and D_2O and 3σ for metal ions) and nuclear density maps (green; 1.6σ contour level). (*b*) OMIT $F_o - F_c$ nuclear density map (magenta; 4σ contour level) for the O5 D atom and $2F_o - F_c$ nuclear density map (green; 2σ level) for His54 and D_2O. Hydrogen bonds made by the O5 hydroxyl group are shown as blue dotted lines.

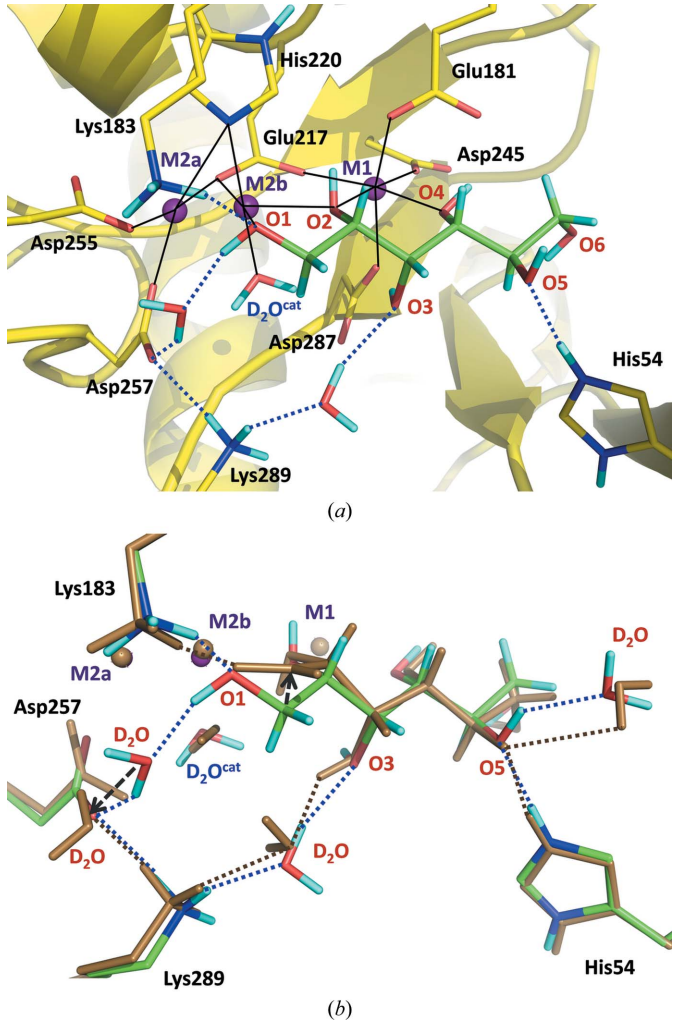

Figure 3
(*a*) Active site of XI with bound sorbitol. Coordination bonds made by Ni^{2+} ions are shown as black dashed lines. (*b*) Superposition of the active sites with sorbitol and linear glucose. Significant structural differences are indicated by black dashed arrows. Sorbitol, residues and D_2O from XI-Ni_2-Sorbitol_xn are colored by atom type, while atoms of the linear glucose complex are shown in light brown. D atoms are colored cyan; H atoms are omitted for clarity. Lys183, Lys289 and His54 are protonated, each carrying a positive charge. Hydrogen bonds are shown as dotted blue and brown lines.

xylitol (XI-Mg_2-Xylitol_x) at basic pH. At basic pH xylitol is positioned in the active site in much the same fashion as at acidic pH, although some details differ. In particular, the water-mediated interaction with Asp257 is absent in XI-Mg_2-Xylitol_x and in our XN structure with linear glucose (Kovalevsky *et al.*, 2010), both of which were obtained at pH 7.7. It is possible that the acidic pH of XI-Ni_2-Sorbitol_xn induces the capture of the extra water molecule by the active site. This additional water molecule would appear to mediate additional contacts between sorbitol and XI residues and improves the inhibitor binding compared with that at basic pH. The absence of this water molecule within hydrogen-bonding distance of the substrate in the linear glucose structure may be a result of higher pH, but can also be explained by the lack of an H atom on the O1 carbonyl O atom of linear glucose (Fig. 3*b*). Thus, the establishment by sorbitol of additional interactions with the active-site residues at low pH should increase its binding affinity for XI and hence may explain why the polyols have increased inhibitory potency under acidic conditions compared with basic conditions (van Bastelaere *et al.*, 1991).

It is instructive to compare the binding of the polyol inhibitor and the linear substrate to the active site of XI at acidic pH and basic pH, respectively, at the atomic level based on the XN structures (Fig. 3*b*). Sorbitol and linear glucose superimpose very well except for the different locations of their C1 atoms, which can be explained by the sp^3 hybridization of the C1 atom of the inhibitor and the sp^2 hybridization in the substrate. However, the O1 atoms of both sugars occupy the same positions and form hydrogen bonds to Lys183. The O3 and O5 hydroxyl groups are hydrogen bonded to D_2O molecules, but the waters have opposite orientations toward sorbitol and linear glucose.

There were also differences in the locations of the metal cations in XI-Ni_2-Sorbitol_xn and XI-Mg_2-Xylitol_x. In both structures metal cations are tightly bound at M1 with low *B* factors. However, in XI-Mg_2-Xylitol_x the electron density at M2 is weak and the *B* factor for the Mg^{2+} ion is an order of magnitude higher than for that at site M1. It would appear that Mg^{2+} at M2 is not constrained to two subsites M2a and M2b as in XI-Ni_2-Sorbitol_xn, but is rather highly mobile at room temperature. We conclude that these subsites can only be significantly occupied at room temperature by transition metals that, unlike Mg^{2+}, can form strong coordination bonds or at low temperature as observed by others (Lavie *et al.*, 1994; Allen *et al.*, 1995; Fenn *et al.*, 2004; Katz *et al.*, 2006; Toteva *et al.*, 2011). This has important implications for the isomerization step and inhibition. A metal ion should occupy subsite M2b, at which it is close enough to the catalytic water (D_2O^{cat}) and the linear substrate to sufficiently polarize their O—H bonds and initiate the isomerization, but it may not have a significant stabilizing effect on the positioning of the O1 atom of a bound sugar.

In summary, we have found that at low pH a polyol forms extra interactions with XI residues that are not observed under basic (physiological) conditions. We have also directly observed protonation of the O5 atom of the inhibitor that makes an important hydrogen bond with His54, while this O atom lacks a D atom in XN structures with linear glucose and xylulose. These observations may prove useful in efforts to re-engineer the XI active site so that it has a lower affinity for polyol inhibitors.

AYK and ZF were partly supported by a DOE-OBER grant to the Neutron Protein Crystallography Station at LANSCE. AYK was partly supported by LANL LDRD Exploratory Research grant 20120256ER. ZF was partially funded by LANL LDRD Early Career Grant 20110535ER. BLH was supported by NSF 446218. VTF and SAM acknowledge support from EPSRC under grants GR/R47950/01, GR/R99393/01 and EP/C015452/1. PL was partly supported by an NIH–NIGMS-funded consortium (1R01GM071939-01) between ORNL and LBNL to develop computational tools for neutron protein crystallography.

References

Adams, P. D., Mustyakimov, M., Afonine, P. V. & Langan, P. (2009). *Acta Cryst.* D**65**, 567–573.
Allen, K. N., Lavie, A., Farber, G. K., Glasfeld, A., Petsko, G. A. & Ringe, D. (1994). *Biochemistry*, **33**, 1481–1487.
Allen, K. N., Lavie, A., Petsko, G. A. & Ringe, D. (1995). *Biochemistry*, **34**, 3742–3749.
Asbóth, B. & Náray-Szabó, G. (2000). *Curr. Protein Pept. Sci.* **1**, 237–254.
Bastelaere, P. van, Vangrysperre, W. & Kersters-Hilderson, H. (1991). *Biochem. J.* **278**, 285–292.
Bhosale, S. H., Rao, M. B. & Deshpande, V. V. (1996). *Microbiol. Rev.* **60**, 280–300.
Callens, M., Kersters-Hilderson, H., van Opstal, O. & De Bruyne, C. K. (1986). *Enzyme Microb. Technol.* **8**, 696–700.
Carrell, H. L., Glusker, J. P., Burger, V., Manfre, F., Tritsch, D. & Biellmann, J. F. (1989). *Proc. Natl Acad. Sci. USA*, **86**, 4440–4444.
Carrell, H. L., Hoier, H. & Glusker, J. P. (1994). *Acta Cryst.* D**50**, 113–123.
Emsley, P., Lohkamp, B., Scott, W. G. & Cowtan, K. (2010). *Acta Cryst.* D**66**, 486–501.
Fenn, T. D., Ringe, D. & Petsko, G. A. (2004). *Biochemistry*, **43**, 6464–6474.
Jänis, J., Pasanen, S., Rouvinen, J. & Vainiotalo, P. J. (2008). *Mass Spectrom.* **43**, 1376–1380.
Katz, A. K., Li, X., Carrell, H. L., Hanson, B. L., Langan, P., Coates, L., Schoenborn, B. P., Glusker, J. P. & Bunick, G. J. (2006). *Proc. Natl Acad. Sci. USA*, **103**, 8342–8347.
Kovalevsky, A. Y., Hanson, L., Fisher, S. Z., Mustyakimov, M., Mason, S. A., Forsyth, V. T., Blakeley, M. P., Keen, D. A., Wagner, T., Carrell, H. L., Katz, A. K., Glusker, J. P. & Langan, P. (2010). *Structure*, **18**, 688–699.
Kovalevsky, A. Y., Hanson, B. L., Mason, S. A., Yoshida, T., Fisher, S. Z., Mustyakimov, M., Forsyth, V. T., Blakeley, M. P., Keen, D. A. & Langan, P. (2011). *Angew. Chem. Int. Ed. Engl.* **50**, 7520–7523.
Kovalevsky, A. Y., Katz, A. K., Carrell, H. L., Hanson, L., Mustyakimov, M., Fisher, S. Z., Coates, L., Schoenborn, B. P., Bunick, G. J., Glusker, J. P. & Langan, P. (2008). *Biochemistry*, **47**, 7595–7597.
Lavie, A., Allen, K. N., Petsko, G. A. & Ringe, D. (1994). *Biochemistry*, **33**, 5469–5480.
Madhavan, A., Tamalampudi, S., Srivastava, A., Fukuda, H., Bisaria, V. S. & Kondo, A. (2009). *Appl. Microbiol. Biotechnol.* **82**, 1037–1047.
Madsen, A. Ø., Mason, S. & Larsen, S. (2003). *Acta Cryst.* B**59**, 653–663.

Maris, A. J. van, Winkler, A. A., Kuyper, M., de Laat, W. T., van Dijken, J. P. & Pronk, J. T. (2007). *Adv. Biochem. Eng. Biotechnol.* **108**, 179–204.
Matsushika, A., Inoue, H., Kodaki, T. & Sawayama, S. (2009). *Appl. Microbiol. Biotechnol.* **84**, 37–53.
Parachin, N. S. & Gorwa-Grauslund, M. F. (2011). *Biotechnol. Biofuels*, **4**, 9.
Pflugrath, J. W. (1999). *Acta Cryst.* D**55**, 1718–1725.
Sheldrick, G. M. (2008). *Acta Cryst.* A**64**, 112–122.
Sudfeldt, C., Schäffer, A., Kägi, J. H., Bogumil, R., Schulz, H. P., Wulff, S. & Witzel, H. (1990). *Eur. J. Biochem.* **193**, 863–871.
Tanino, T., Hotta, A., Ito, T., Ishii, J., Yamada, R., Hasunuma, T., Ogino, C., Ohmura, N., Ohshima, T. & Kondo, A. (2010). *Appl. Microbiol. Biotechnol.* **88**, 1215–1221.
Toteva, M. M., Silvaggi, N. R., Allen, K. N. & Richard, J. P. (2011). *Biochemistry*, **50**, 10170–10181.
Van Vleet, J. H. & Jeffries, T. W. (2009). *Curr. Opin. Biotechnol.* **20**, 300–306.
Whitlow, M., Howard, A. J., Finzel, B. C., Poulos, T. L., Winborne, E. & Gilliland, G. L. (1991). *Proteins*, **9**, 153–173.
Wilkinson, C., Khamis, H. W., Stansfield, R. F. D. & McIntyre, G. J. (1988). *J. Appl. Cryst.* **21**, 471–478.
Winn, M. D. *et al.* (2011). *Acta Cryst.* D**67**, 235–242.